Macromolecules

pubs.acs.org/Macromolecules Article

Using Liquid Crystals to Probe the Organization of Helical Polypeptide Brushes Induced by Solvent Pretreatment

Michael Tsuei, Hai Tran, Sangchul Roh, Christopher K. Ober,* and Nicholas L. Abbott*

Cite This: *Macromolecules* 2021, 54, 7786−7795 Read Online

ACCESS | Metrics & More | Article Recommendations | Supporting Information

ABSTRACT: Grafted polymer brushes form the basis of a versatile class of surfaces with properties that can be tailored via choice of the chemical functional groups or architecture of the grafted polymers. Here, we explore how treatment by solvents can program the organization of homopolymer brushes comprising helical poly(γ-benzyl-L-glutamate) (PBLG) and how the orientational behavior of liquid crystals (LCs) contacted with the brushes can provide fresh insights into brush organization. We treated PBLG brushes with either good (chloroform) or poor (acetone) solvents to form collapsed or teepee-like grafted polymer organizations, respectively. When supported on PBLG brushes with thicknesses [determined by atomic force microscopy (AFM)] of 50 nm, we found that collapsed and teepee-like brushes induced planar (parallel to surface) and homeotropic (perpendicular to surface) orientations of nematic LCs, respectively. By preparing solvent-pretreated brushes with a range of thicknesses (12−140 nm), and by combining insights based on AFM, Fourier-transform infrared spectroscopy and LCs, we found that a continuous change in tilt of the LC is accompanied by a continuous change in tilt of the PBLG chains, as influenced by the teepee-like organization. The role of PBLG chain orientation in dictating the LC orientation was confirmed by additional experiments in which PBLG brushes were thermally denatured. Finally, when using mixed solvents (mixtures of chloroform and acetone) to manipulate the PBLG brush organization, we observed LCs to exhibit patterned orientations on the micrometer scale, consistent with patterned orientations of the PBLG chains imprinted by droplets formed during the mixed solvent drying process. Overall, these results expand our understanding of the range of PBLG brush organizations that can be induced by solvent pretreatment and demonstrate the utility of LCs for imaging PBLG chain orientation within brushes.

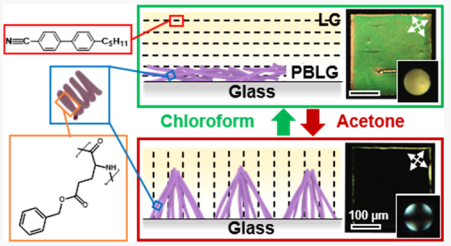

1. INTRODUCTION

Grafted polymer brushes offer the basis of smart surfaces that respond to external stimuli such as electric fields, solvents, and temperature.[1−6] Their stimuli responsiveness has led to their application in a range of contexts including as organic diodes and transistors,[7−9] actuators,[10,11] and platforms for molecular recognition.[12] Because the organization of the end-attached chains within the brush plays a key role in defining their properties (e.g., electrooptical[13] and electromechanical[4]), identifying versatile methods that enable switching of polymer brush organization is central to realizing the full potential of smart surfaces based on these materials.

In contrast to coil-type polymer brushes that are flexible and assume a limited range of surface organizations, polypeptide brushes, which can possess high persistence lengths due to their secondary structure (α-helical or β-sheet conformations), provide access to more complex, orientationally ordered surface states.[14,15] In particular, surface-grafted poly(γ-benzyl-L-glutamate) (PBLG; Figure 1a) has been studied extensively due to its stable helical structure and associated electrical properties (e.g., piezoelectric[16] and inverse piezoelectric[4] properties). In this work, we explore how solvent-induced organizations of PBLG brushes influence the orientational ordering of liquid crystals (LCs) placed onto these surfaces, and how the LC ordering behavior can feed back to provide new insights into the solvent-induced organization of the brushes.

A range of approaches have been reported previously to drive changes in the orientational states and properties of grafted polypeptide brushes. For example, Machida et al.[17] demonstrated that the net dipole moments of PBLG brushes could be tuned by using applied electric fields. Alternatively, Yang et al.[18] demonstrated that poly(β-benzyl-L-aspartate) brushes could be reversibly switched between left-handed and right-handed α-helical structures by exposure to vapors of organic solvents. The origin of the screw-sense inversion was attributed to small changes in the strength of the dipole−dipole interactions between the amide backbone and ester side chains induced by the solvent vapor. Of particular relevance to our study, Wang et al.[5,19] reported that the orientations of surface-grafted PBLG chains can be switched via "solvent quenching", a process wherein a grafted brush is first swollen

Received: May 24, 2021
Revised: July 21, 2021
Published: August 30, 2021

https://doi.org/10.1021/acs.macromol.1c01125
Macromolecules 2021, 54, 7786−7795

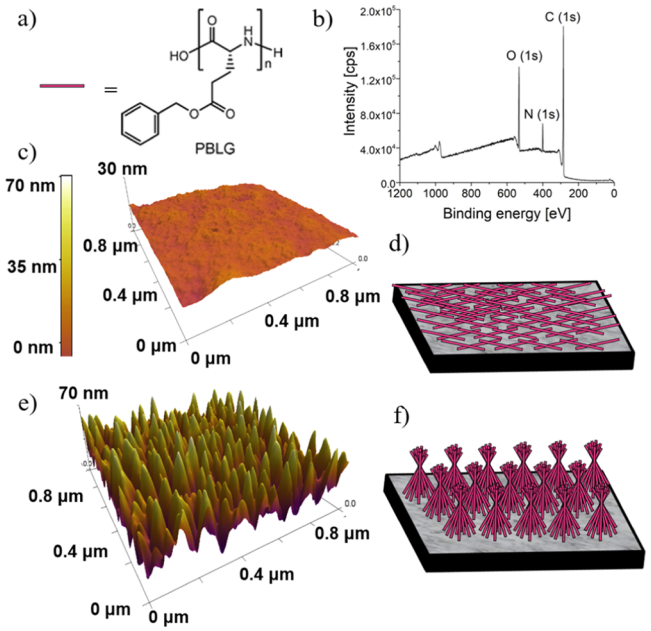

Figure 1. (a) Molecular structure of PBLG. (b) XPS survey spectrum of PBLG brushes revealing presence of C, O, and N. (c,e) AFM 3D height profiles of PBLG brushes and (d,f) representative schematic illustrations of PBLG brushes adopting a (c,d) collapsed conformation and (e,f) quenched conformation.

with a good solvent such as chloroform, rapidly transferred into a poor solvent for PBLG such as acetone and then dried. The process results in the formation of teepee-like assemblies comprising clusters of PBLG chains. The solvent quenching process enables brushes to be switched between a "collapsed" state ($\theta = 49 \pm 2°$, where θ is the average angle between the helix axis of PBLG and the surface normal), and a "quenched" state (teepee-like assemblies; $\theta = 3 \pm 2°$). In this work, we build from this prior study by exploring a wider range of solvent conditions (including mixed solvents) and by characterizing the orientations of LCs on solvent-imprinted PBLG brush organizations.

A key challenge underlying the rational design of smart surfaces based on polypeptide brushes is characterization of the organization of the brushes. In past studies, the out-of-plane orientations of PBLG chains were characterized by Fourier transform infrared (FTIR) spectroscopy,[20−22] which provides average molecular orientations of the grafted chains, and atomic force microscopy (AFM),[5,15] which probes mesoscale surface topography. While these past studies provided important insights in brush organization, they also highlight the limitations of FTIR and AFM methods. FTIR probes the tilt angles of polymer chains averaged across large (mm^2) surface areas and, therefore, does not provide insights into sub-millimeter scale, spatial variations (e.g., patterning) of brush organization. In contrast, AFM reports the mesoscale surface structure, but rarely provides molecular-scale information when used with brushes.[23] These attributes, when combined, make characterization of the molecular-level organization of brushes within micrometer-scale patterns difficult to perform: FTIR does not have spatial resolution, and patterns of topography identified by AFM are challenging to interpret in terms of molecular orientation. Here, we explore how PBLG brush organization impacts LC ordering and then demonstrate the utility of LCs in probing the organization of patterned polymer brushes observed with mixed solvent pretreatment.

The orientational ordering and fluidity of LCs (e.g., nematic LCs) is known to permit amplification of molecular and nanoscopic structures at interfaces into easily visualized and quantifiable changes in optical properties.[24−27] Past studies have shown that surfaces can align LCs via interactions such as van der Waals interactions,[28,29] steric interactions,[30,31] and electrical double-layer interactions.[32] Polymer brushes formed on surfaces have also been reported to impact the orientations of LCs.[33−35] For example, Li et al.[34] demonstrated that the orientations of LCs in contact with poly(6-(4-methoxy-azobenzene-4′-oxy)hexyl methacrylate) (PMMAZO) brushes (~3−13 nm thick) could be controlled by varying the grafting density of the brush. At high grafting densities, the mesogenic side chains aligned tangentially with respect to the substrate, resulting in either tangential (planar) or tilted alignment of the LCs. In contrast, at low grafting densities, the mesogenic side chains aligned perpendicular to the substrate, resulting in perpendicular (homeotropic) alignment of the LCs. Past studies have also explored interactions of LCs supported on surfaces decorated with PBLG molecules that were grafted via their carbonyl end groups.[17,36−38] These studies revealed that the presence of a grafted PBLG brush (and its large dipole moment) modulated the response of the LC to an electric field. In our study, we reveal that solvent pretreatment of a PBLG brush, which changes PBLG chain orientation, can have a profound influence on the ordering of LCs supported on PBLG brushes.

The organization of this paper is as follows. First, we report experiments that were performed to explore how solvent-induced changes in the ordering of PBLG brushes impact the orientations of supported LCs. Second, to provide insight into our observations, we prepared brushes that differed in thickness, and we characterized the solvent-induced changes in organization by using FTIR spectroscopy, AFM and LCs. These measurements lead to the key insight that the orientational order of the LC is correlated closely to the tilt of PBLG chains, as regulated by the formation of teepee-like assemblies. We also report how thermal denaturation of the PBLG changes both PBLG and LC ordering. Finally, we explore PBLG organizations induced by pretreatment with mixtures of good and poor solvents and we use LCs to unmask observations of spontaneous surface patterning of the PBLG tilt angle induced by the drying process. Overall, the results presented in this paper advance our understanding of the diversity of brush organizations that can be induced by solvent treatment and reveal the utility of LCs as probes of the organization of this class of polymer brush.

2. EXPERIMENTAL SECTION

2.1. Materials. Anhydrous toluene, γ-benzyl L-glutamate, and triphosgene were purchased from Sigma-Aldrich and used as received. 3-Aminopropyldimethyl-ethoxysilane (APDMES) was purchased from Gelest. Copper tape (882-L COPPER) was purchased from Lamart Co. Deionized water with a resistivity of 18.2 MΩ cm at 25 °C was obtained from a Millipore Milli-Q Synthesis A10 system. Tetrahydrofuran was distilled over sodium. All other solvents were used as received from Fisher Scientific. Si(100) double-sided polished wafers were from WRS Materials. Cantilevers were purchased from Applied NanoStructures, Inc. (ACCESS-NC). The nematic LC, 4-cyano-4′-pentylbiphenyl (5CB), was purchased from HCCH (Jiangsu Hecheng Display Technology Co., Ltd). Chloroform and hexane were purchased from VWR Chemicals BDH.

https://doi.org/10.1021/acs.macromol.1c01125
Macromolecules 2021, 54, 7786−7795

Scheme 1. PBLG Brush Synthesis Procedure

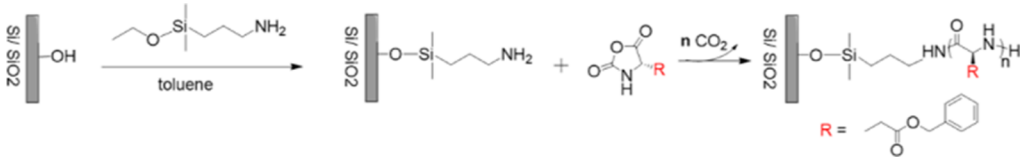

2.2. Synthesis of PBLG Brushes. γ-Benzyl L-glutamate *N*-carboxyanhydride (NCA monomer) was synthesized by using a published procedure.[39] Glass slides and silicon wafers were cut into 12 mm × 25 mm pieces and cleaned in a solution of 70% (v/v) H_2O, 15% (v/v) HCl (ACS reagent, 37%), and 15% H_2O_2 (ACS reagent, 30%) at 50 °C for 1 h. The slides and wafers were then washed with methanol, dried with nitrogen gas, and placed in an oven at 110 °C for 10 min. Subsequently, the slides and wafers were oxidized using a Harrick Plasma Cleaner for 10 min. Processed glass slides and silicon wafers were immersed in toluene solution containing APDMES (initiator; 120 mM) at room temperature for 16 h. The substrates were then washed with toluene and methanol before drying with nitrogen gas.

10 mg of the NCA monomer was added and spread across the bottom of a 10 mL glass beaker. An initiator-immobilized substrate was fixed on top of the beaker with copper tape. The beaker and the substrate were then put into a glass chamber connected to a Schlenk line. The glass chamber was subsequently evacuated to 500 mTorr and heated in an oil bath to 105 °C for different amounts of time to control polymer brush thickness. After the reaction, the substrate was sonicated in chloroform and blow-dried with nitrogen gas.

2.3. Characterization of PBLG Brushes. Polymer brushes on double-polished wafers were characterized by FTIR spectroscopy (Bruker Optics-Vertex 80v). The spectra were taken in transmission mode and recorded with 4 cm^{-1} resolution and 256 scans. X-ray photoelectron spectroscopy (XPS) measurements were performed with a Surface Science Instruments SSX-100 using a monochromatic Al Kα source (1486.6 eV). Photoelectrons were collected at a 55° emission angle. AFM (Asylum MFP-3D) was used to characterize the surface topography of polymer brushes using AC tapping mode using silicon cantilevers (model: ACCESS-NC).

2.4. Treatment of PBLG Brushes with Good and Poor Solvents. Treatment of all PBLG brushes with single component or mixtures of solvents and poor solvents started with solvation of the brushes in 3 mL chloroform for 2 min. Solvent quenching in acetone required direct transfer of the chloroform-solvated brush into 3 mL acetone for 1 min and subsequent drying via compressed air. Treatment with mixtures of poor solvents involved direct transfer of the chloroform-solvated brush into mixtures of acetone and water for 1 min and subsequent drying using compressed air. Treatment with mixtures of good and poor solvents required direct transfer of solvated brushes into mixtures of chloroform and acetone for 1 min and subsequent drying using compressed air.

2.5. Preparation of Thin LC Films. 20 μm-thick LC films were prepared by pipetting 0.5 μL of LC (i.e. 5CB or MBBA) into the pores of 75 mesh (thickness 20 μm; lateral pore size 285 μm) transmission electron microscopy grids that were supported on the PBLG brushes. Excess LC was then removed via capillary action to produce a LC film with a thickness of 20 μm.

2.6. Optical Microscopy. An Olympus BX41 microscope with 4×, 20×, and 50× objectives, two rotating polarizers, and a Moticam 10.0 MP camera was used for optical microscopy.

2.7. Heating of PBLG Brushes. 130 nm-thick PBLG brushes were prepared and heated to 180 °C for either 0, 4, 15, or 300 min. After heating, the samples were cooled to 25 °C and the surface topography of each brush was measured using AFM. The average PBLG chain tilt angle was measured using FTIR, and the lateral organization of each brush was measured using LCs.

3. RESULTS AND DISCUSSION

3.1. Ordering of LCs on Solvent-Pretreated PBLG Brushes. In our initial experiments, we used the solvent treatment method described by Wang et al.[5] to prepare PBLG brushes that differed in their organization (collapsed vs teepee-like state). We prepared 50 nm-thick polymer brushes (Figure 1a; thickness determined via AFM), with grafting density and PBLG molecular weight calculated to be 0.397 chains/nm^2 and 77,307 g/mol, respectively (see Section S1), via surface-initiated ring opening polymerization (Scheme 1).

The presence of the PBLG brushes on glass substrates was verified via XPS. The measured elemental composition (see Figure 1b) was consistent with the calculated composition of PBLG: measured (calculated) 15.9 ± 0.8% (18.8%) oxygen, 78 ± 1.4% (75%) carbon, and 6.1 ± 0.7% (6.3%) nitrogen. When the chloroform-treated PBLG brushes were dried with compressed air, AFM measurements confirmed that the brushes adopted a collapsed conformation (Figure 1c,d). Instead, if the brushes in chloroform were directly transferred into acetone and subsequently dried with compressed air, the PBLG chains formed teepee-like assemblies, hereafter referred to as a quenched organization (Figure 1e,f).

We estimated the average tilt angles of the PBLG chains in the collapsed and quenched brushes using FTIR spectroscopy in transmission mode. We calculated the dichroic ratio from two characteristic amide peaks (amide I-1654 cm^{-1} and amide II-1550 cm^{-1}) in the absorbance spectra and used it to estimate the average tilt angles (with respect to the surface normal) of the collapsed and quenched PBLG brushes to be 43.0 ± 0.3 and 20.2 ± 0.8°, respectively (see Section S2). We note here that the solvent-induced PBLG tilt angles measured in our experiments differ from prior studies (see Introduction). The difference likely arises from variation in the grafting density of the PBLG brushes, which in turn arises from the use of distinct substrates in the two sets of experiments (e.g., glass vs alumina or gold) and differences in the procedures used to deposit the initiator (monolayers of ethoxysilane[40−42] in the studies reported here and multilayers of di- and tri-ethoxysilanes[43,44] in the prior studies).

Next, we sought to determine if the two states of the PBLG brush would lead to differences in the ordering of supported LCs. We placed 20 μm-thick metal grids onto either collapsed or quenched 50 nm-thick PBLG brushes and filled the grids with nematic 5CB (Figure 2a). When viewed between crossed polarizers in transmission mode, the LC films supported on the collapsed brushes exhibited a bright optical appearance (Figure 2b). From the optical interference colors, which were interpreted using a Michel−Levy chart, we calculated the LC tilt angle at the LC-brush interface (averaged over three samples) to be 87 ± 2° (see Section S3), indicating tangential (planar) LC alignment (Figure 2b,d). In contrast, LCs supported on quenched brushes exhibited a dark optical texture (Figure 2c) consistent with perpendicular (homeotropic) LC alignment at the LC-brush interface (Figure 2c,e).

https://doi.org/10.1021/acs.macromol.1c01125
Macromolecules 2021, 54, 7786−7795

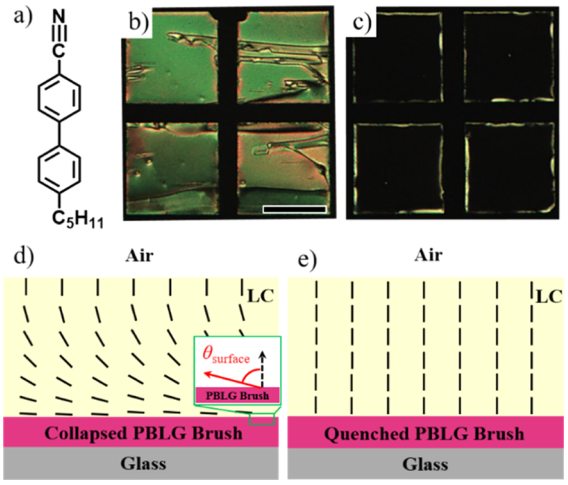

Figure 2. (a) Molecular structure of 5CB. (b,c) Optical micrographs (crossed polarizers) and (d,e) corresponding schematic illustrations of LC thin films on 50 nm-thick PBLG brushes in a (b,d) collapsed and (c,e) quenched conformation. Scale bar in micrograph is 200 μm.

These observations suggest that LCs can amplify different PBLG brush organizations into optical signals via their ordering. We verified also that the LC was a poor solvent for PBLG and did not change the organization of the PBLG brushes upon contact. Specifically, we pretreated brushes to create collapsed or quenched states, incubated the brushes against LC for 15 min, removed the LC using acetone (a good solvent for LC and a poor solvent for PBLG) and performed FTIR on the substrates after drying with compressed air. Measurements of PBLG brush orientation before and after incubation in LC revealed no significant change in the average tilt angles (43 ± 1° from the surface normal for the collapsed and 19 ± 1° for the quenched brush) of the PBLG chains (see Section S4).

Next, we sought to determine if the difference in LC orientation reported above was a result of the PBLG changing the lowest free energy orientation of the LC (so-called easy axis) or changing the free energy cost required to reorient the LCs at the PBLG brush interface (surface anchoring energy; see Sections S5 and S6). We differentiated between the two mechanisms by confining a 4 μm-thick LC film between two acetone-quenched 50 nm-thick PBLG brushes (see Section S6). Observation of LCs in contact with the quenched brushes (crossed polarizers) revealed a dark optical texture indicative of homeotropic LC alignment (see Section S6). In contrast, when observed between crossed polarizers, 4 μm-thick LC films confined between chloroform-collapsed brushes exhibited a bright optical texture indicative of an alignment of the LCs that was not homeotropic (see Section S6). These observations indicate that a change in the organization of PBLG brushes induces a change in the easy axis of the LCs.

3.2. PBLG Brushes that Differ in Thicknesses. To provide additional insight into the molecular-level mechanism by which the organization of solvent-treated PBLG brushes trigger distinct orientations of LCs, we prepared PBLG brushes with thicknesses ranging from 140 to 12 nm. After pretreatment with either chloroform or acetone, we determined the height profiles of the brushes using AFM (see Figure 3a–h and Section S7). In Figure 3a–h, we summarize differences found in the thickest (140 nm) and thinnest (12 nm) PBLG brushes following solvent treatment (additional data for brushes of intermediate thickness can be found in Section S7).

AFM measurements of the 140 nm-thick PBLG brushes (Figure 3a–d) revealed a striking difference in roughness of the brush following chloroform or acetone treatment. Similar to the 50 nm-thick brushes (Figure 1), the acetone-treated 140 nm-thick brushes exhibited topography that was consistent with the presence of a teepee-like organization with a root-mean-square (rms) roughness [calculated using AFM analysis software (Gwyddion) over an area of 1 μm^2] of 33.6 ± 1.4 nm, whereas the chloroform-treated brushes were smooth in comparison with an rms roughness of 2.1 ± 0.2 nm. In contrast to the thick brushes, the topography of the 12 nm-thick PBLG brushes obtained from AFM (Figure 3e–h) exhibited a minor change with solvent treatment, such that the rms roughness of the chloroform and acetone-treated brushes were 2.3 ± 0.4 and 3.1 ± 0.3 nm, respectively. Close inspection of the AFM 3D height profiles revealed that the chloroform and acetone-treated 12 nm-thick brushes both exhibited topography characteristic of teepee-like organizations, with the areal densities of teepee-like assemblies varying from 53 ± 7 teepees/μm^2 (chloroform) to 205 ± 12 teepees/μm^2 (acetone). Additional measurements reported below using LCs and FTIR spectroscopy support these conclusions.

Next, we optically characterized LC films (between crossed polarizers) supported on 12 or 140 nm-thick PBLG brushes treated with either chloroform or acetone. LCs supported on 140 nm-thick PBLG brushes exhibited planar (Figure 3i) or homeotropic (Figure 3j) alignment on brushes treated with chloroform or acetone, respectively. In contrast, LCs supported on 12 nm-thick PBLG brushes exhibited homeotropic alignment independent of the solvent treatment (Figure 3k,l). These results obtained using LCs correlate closely with our proposed interpretation of the AFM measurements (specifically, that teepee-like organization is present in the thin PBLG brushes independent of solvent treatment). We note, however, that the LC response to the PBLG brush organization is not controlled by surface roughness. This is supported by our observation that chloroform-treated 140 nm-thick brushes, which exhibit an rms roughness of 2.1 ± 0.2 nm, induces planar LC alignment, while chloroform-treated 12 nm-thick brushes, which exhibit an rms roughness of 2.3 ± 0.2 nm, induce homeotropic alignment. Prior studies[45] have reported that surface roughness can influence the orientations of LCs, but those studies employed surfaces with rms roughness values that were much larger than 2 nm.

Measurements of the average PBLG tilt angles (obtained by FTIR spectroscopy) following solvent treatment (Figure 4a), revealed that PBLG brushes exhibited average PBLG chain tilts that changed as a function of PBLG brush thickness (12, 25, 50, and 140 nm; Figure 4a–d). Specifically, acetone-treated brushes exhibited a decrease in average PBLG chain tilt angle from the surface normal (26 ± 1 to 15 ± 2°) with increasing brush thickness, whereas chloroform-treated brushes exhibited an increase in PBLG chain tilt angle (35 ± 1 to 45 ± 1°) with increasing brush thickness (Figure 4e). Significantly, the tilt angles of the PBLG brushes appear to converge in the limit of decreasing brush thickness. This observation indicates that the range of tilt angles that PBLG chains can access in response to good and poor solvent treatment decreases with decreasing brush thickness. Additionally, this observation is supported by our AFM measurements with thin PBLG brushes (topographical features independent of solvent pretreatment; Figure

https://doi.org/10.1021/acs.macromol.1c01125
Macromolecules 2021, 54, 7786–7795

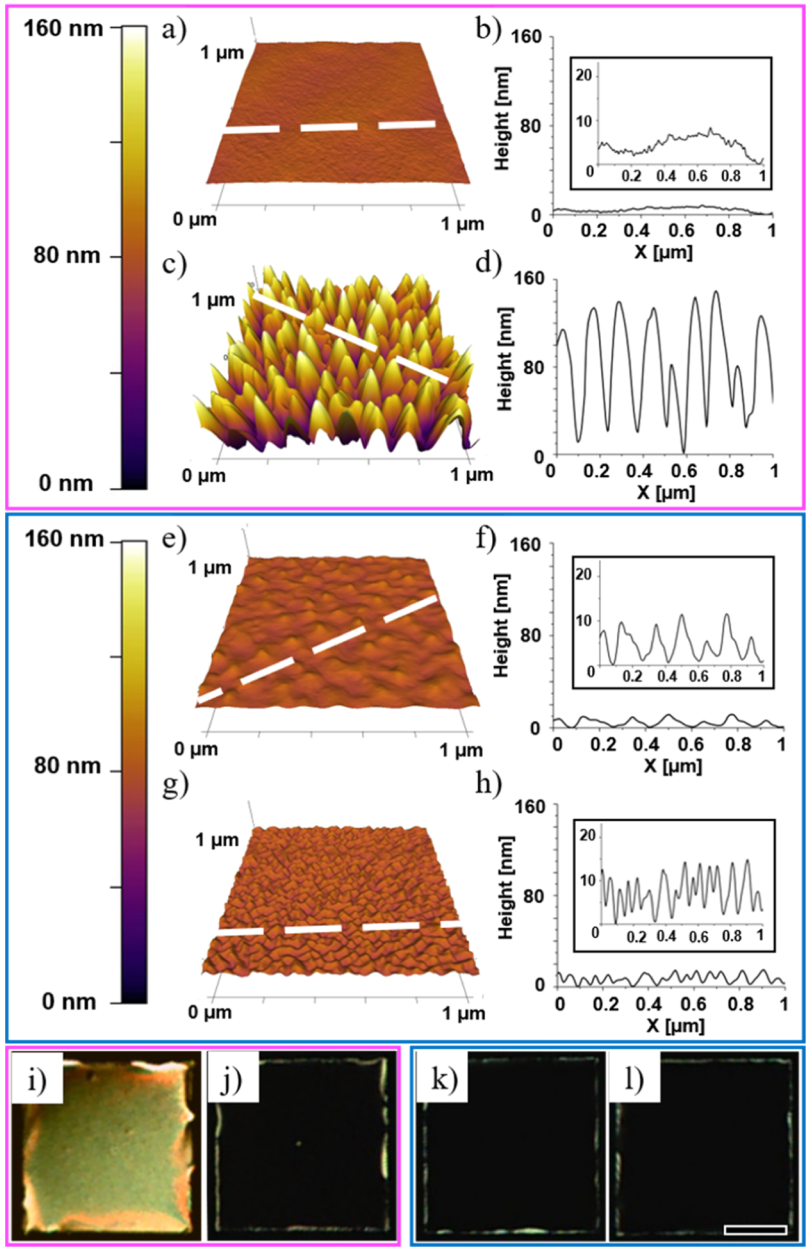

Figure 3. (a,c,e,g) 3D and (b,d,f,h) 2D height profiles of (a−d) 140 nm- and (e−h) 12 nm-thick PBLG brushes measured via AFM and (i−l) corresponding optical micrograph (crossed polarizers) of LC thin films on (i,j) 140 nm- and (k,l) 12 nm-thick PBLG brushes treated with (a,b,e,f,i,k) chloroform and (c,d,g,h,j,l) acetone. Dotted white lines show a cross-section of the 3D profile to generate 2D height profiles. Black insets (b,f, h) show zoomed-in 2D height profiles. Scale bar in the micrograph is 100 μm.

3a−h and Section S7) and LC orientations (homeotropic LC orientation independent of solvent pretreatment; Figure 3k,l).

Figure 4e,f summarizes the overall trends in the PBLG tilt angle and LC tilt angle measured on solvent-treated PBLG brushes as a function of brush thickness. The LC tilt angles were quantified by using the interference colors (see Section S8) to determine the optical retardance. Inspection of these figures revealed that, for chloroform-treated brushes, both the PBLG tilt angle and LC tilt angles increased with PBLG brush thickness (Figure 4f, green triangles). In contrast, for acetone-treated brushes, the PBLG tilt angles decreased with increasing PBLG brush thickness (diverging from the tilt angles of the brushes treated with chloroform), and the LC exhibited homeotropic alignment (Figure 4f, red circles).

The results in Figure 4 reveal a close correlation between the PBLG tilt angle and LC orientation. To understand the possible origins of the intermolecular interactions that couple the LC orientations and PBLG chain organization, we compared the orientational responses of 5CB on the PBLG brushes to *N*-(4-methoxybenzylidene)-4-butylaniline (MBBA) (see Section S9). In contrast to 5CB, which possesses positive dielectric anisotropy and positive anisotropic polarizability, MBBA possesses negative dielectric anisotropy and positive anisotropic polarizability.[28,46,47] However, we found that MBBA and 5CB exhibited the same orientational response to the PBLG brushes, thus suggesting that dispersion interactions rather than dipolar interactions dominate the coupling of the organization of the PBLG brush to the LCs (see Section S9).

https://doi.org/10.1021/acs.macromol.1c01125
Macromolecules 2021, 54, 7786−7795

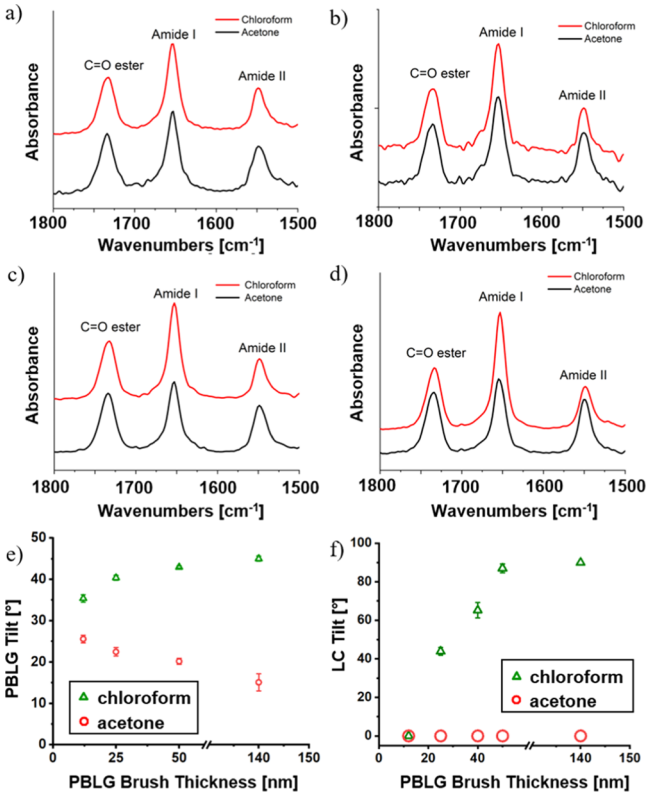

Figure 4. (a–d) FTIR spectra of (a) 12, (b) 25, (c) 50, and (d) 140 nm-thick PBLG brushes treated with chloroform (red) and acetone (black). The labeled peaks are amide I (1654 cm^{-1}, backbone carbonyl stretching), amide II (1550 cm^{-1}, C–N stretching) of α-helical secondary structure, and the ester side chain (1734 cm^{-1}). (e) Average PBLG chain tilt angles from the surface normal as a function of PBLG brush thickness for chloroform (green triangles) and acetone-treated (red circles) PBLG brushes. (f) LC tilt angles from the surface normal at the PBLG brush surface as a function of PBLG brush thickness for chloroform (green triangles) and acetone-treated (red circles) PBLG brushes. Data points show mean values, and the error bars represent 1 standard deviation (n = 3).

3.3. Thermal Denaturation of PBLG Brushes. The results above lead to the proposal that the orientation of the PBLG chains (which form helices by intramolecular hydrogen bonding; Figure 5a) within the brush program the orientation of the LC. To further test this proposal, we thermally denatured PBLG brushes.[5,17,48] Specifically, after solvent quenching 130 nm-thick PBLG brushes in acetone, we heated the brushes to 180 °C for 0 min (Figure 5b,f), 4 min (Figure 5c,g), 15 min (Figure 5d,h), and 300 min (Figure 5e,i). Prior to contacting the heat-treated surface with LC, we rinsed the surfaces with chloroform and then acetone to remove any PBLG chains that were no longer tethered to the substrate. As shown below by FTIR spectroscopy, this solvent treatment step does not renature the PBLG chains. After heat treatment, we probed changes in PBLG structure via AFM (Figure 5b–e), LCs (Figure 5f–i), and FTIR (Figure 5j,k).

AFM measurements at each time step showed a continuous decrease in surface topography associated with the initial teepee-like organization of the PBLG brush (Figure 5b–e).[18] LCs supported on PBLG brushes heat-treated for different durations showed a progression of interference colors (Figure 5f–i), which we interpreted using a Michel–Levy chart to correspond to LC tilt angles of 0° at 0 min (Figure 5f), 20 ± 8° at 4 min (Figure 5g), 50 ± 3° at 15 min (Figure 5h), and 89 ± 1° at 300 min (Figure 5i) of heating at 180 °C. FTIR measurements at each time step (Figure 5j) reveal a change in relative intensity of amide I and amide II bands suggestive of an increase in PBLG chain tilt angle with increasing duration of heat treatment (Figure 5k). We note, however, that heating also leads to partial unfolding of the PBLG helices, which we verified through deconvolution of the FTIR spectra to reveal an increase in random coil content (amide I random coil–1680 cm^{-1})[49,50] with increasing heating time (see Section S11). Overall, the relationship between PBLG and LC tilt angles observed during heat treatment is generally similar to that obtained via solvent-treatment of PBLG brushes with different thickness (Figure 4 and Section S10). This similarity reinforces our conclusion that the LCs respond to the orientations of the PBLG molecules within the solvent-treated brushes.

3.4. Reorganization of PBLG Brushes with Mixed Solvents. Next, we investigated whether an expanded diversity of PBLG brush organization might be achieved by using solvent mixtures. Specifically, we investigated PBLG brush organizations that were generated by using mixtures of good (chloroform) and poor (acetone) solvents. We solvated 140 nm-thick PBLG brushes in chloroform and transferred the solvated brushes into solvent mixtures comprising either 10 or 25% v/v chloroform in acetone for 1 min and then dried the samples with a stream of compressed air. FTIR measurements of brushes pretreated with the mixed solvents revealed average PBLG tilt angles (averaged over an area of 79 mm^2) that were intermediate between that obtained using either of the pure solvents (see Table 1 and Section S12).

The results in Table 1 indicate that the average PBLG tilt angle can be changed by choice of the solvent composition. We tested if the correlation between the PBLG tilt angle and LC tilt angle established with pure solvent (Figure 4e,f and Section S10) was also observed when using solvent mixtures. Interestingly, LCs supported on PBLG brushes treated with 10% chloroform in acetone exhibited patterned orientations (Figure 6a). Inspection of Figure 6a revealed (i) large circular homeotropic domains with diameters of 26 ± 3 μm (Figure 6a; yellow-bordered box) and (ii) small circular domains with tilted LC alignment and diameters of 6 ± 4 μm (Figure 6a; red-bordered box). The region inside the small circular domains (red box) revealed an orange optical texture, which corresponds to a LC tilt angle of 55 ± 2° via comparison with the Michel–Levy chart. In comparison, the region immediately outside the circular domains exhibited a dark green optical texture, which corresponds to a LC tilt angle of 48 ± 2°. By using the relationship between PBLG and LC tilt established in Figure 4e,f (see also Section S10), we propose that the PBLG brush pretreated with mixtures comprising 10% chloroform/90% acetone is patterned with domains comprising PBLG tilt angles of 41 ± 0.2° (small circular domains), 40 ± 0.2° (region outside small circular domains), and 15–35° (homeotropic domains). We note that while the difference in PBLG tilt angles inside and outside the small circular domains is small, the interference colors exhibited by the LCs in the two regions are clearly different. Additionally, the area-weighted average tilt angle calculated using these three domains (see Section S13) is 38–40° (depending on the tilt value used in the homeotropic domains), which is generally consistent with that determined via FTIR (37 ± 1°; Table 1). Overall, these observations suggest that LCs can be used to probe PBLG chain tilt angles

https://doi.org/10.1021/acs.macromol.1c01125
Macromolecules 2021, 54, 7786–7795

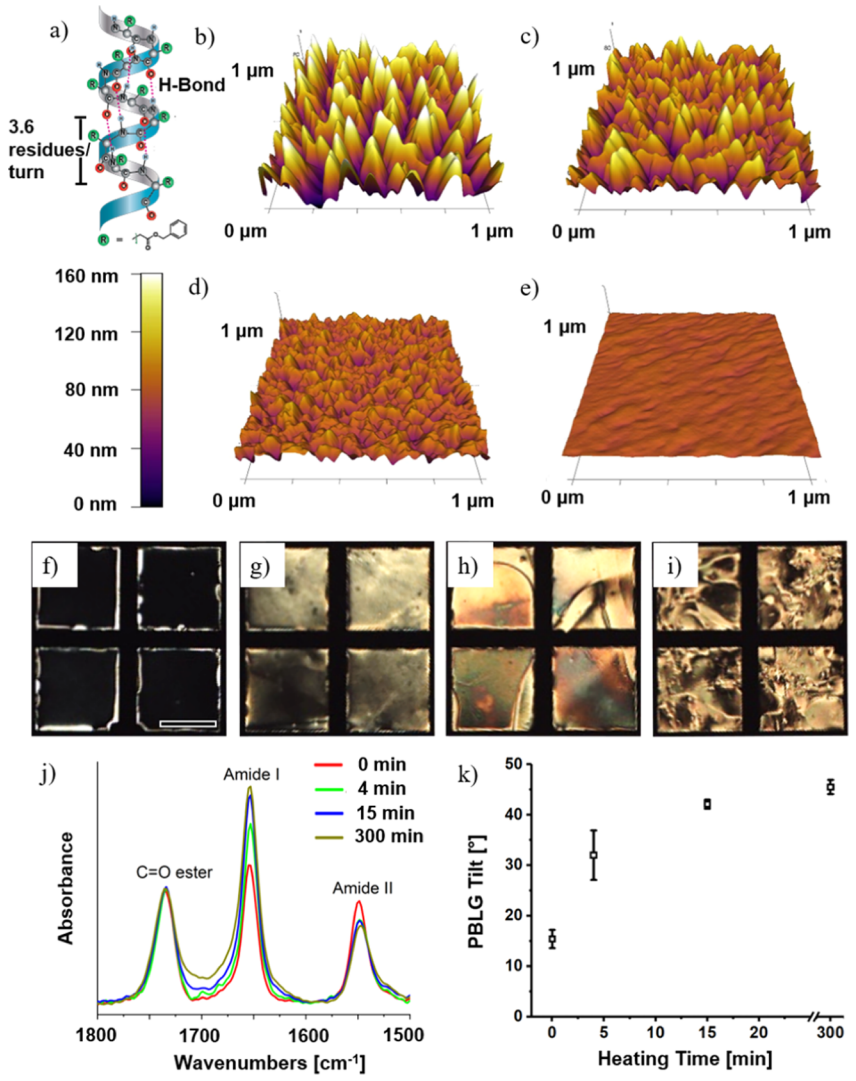

Figure 5. (a) Schematic illustration of PBLG chain, whose rigid helical structure is a result of hydrogen bonds. (b−e) AFM 3D height profiles and (f−i) corresponding micrographs of 20 μm-thick LC films supported on PBLG brushes heated for (b,f) 0, (c,g) 4, (d,h) 15, and (e,i) 300 min. (j) FTIR spectra of acetone-quenched 130 nm-thick PBLG brushes following 0, 4, 15, and 300 min of heating at 180 °C and re-quenching in acetone. The labeled peaks are amide I (1654 cm^{-1}, backbone carbonyl stretching), amide II (1550 cm^{-1}, C−N stretching) of α-helical secondary structure, and the ester side chain (1734 cm^{-1}). (k) Apparent PBLG tilt angles estimated via FTIR as a function of heating time. Scale bar in the micrograph is 200 μm. Data points show mean values, and the error bars represent 1 standard deviation (n = 3).

Table 1. Average Orientations of 140 nm-Thick PBLG Brushes Measured via FTIR Following Treatment with Chloroform−Acetone Mixtures

v/v % chloroform in acetone	PBLG tilt angle (θ) from surface normal
0	15 ± 2
10	37 ± 1
25	39 ± 1
100	45 ± 1

within micrometer-scale domains, which is not easily achieved via either AFM or FTIR spectroscopy.

We also performed AFM measurements of the small circular domains in Figure 6a, which revealed that the circular domains possessed topographical rims (Figure 6c and Section S14). The rims had characteristic heights of 91 ± 17 nm, whereas the apparent thicknesses of the PBLG brushes inside and outside the rings were 45 ± 7 and 25 ± 17 nm, respectively. The presence of the ring hints at a "coffee stain" effect,[51−53] as is often observed when droplets evaporate from surfaces, leading to a local reorganization of the PBLG brushes due to capillary forces and fluid flows associated with the receding solvent contact line.

We also sought to determine if the PBLG brush response to mixed solvent treatment changes with brush thickness. Figure 6b shows the optical map generated by LCs supported on 50 nm-thick brushes treated with a mixture of 10% v/v chloroform in acetone. In contrast to the 140 nm-thick PBLG brush, inspection of Figure 6b reveals a continuous homeotropic orientation of the LCs (dark regions) within which are embedded bright domains with diameters between 2 and 20 μm (Figure 6b; blue-bordered box). Optical retardance measurements revealed that the LC tilt angle at the center of the domains was 39 ± 7°, which corresponds to PBLG tilt angles of 39 ± 1°. AFM measurements revealed circular domains that had elevated topographies (Figure 6d,f and Section S15) and were surrounded by a ring-like region comprising collapsed PBLG. Because the LC assumes an

https://doi.org/10.1021/acs.macromol.1c01125
Macromolecules 2021, 54, 7786−7795

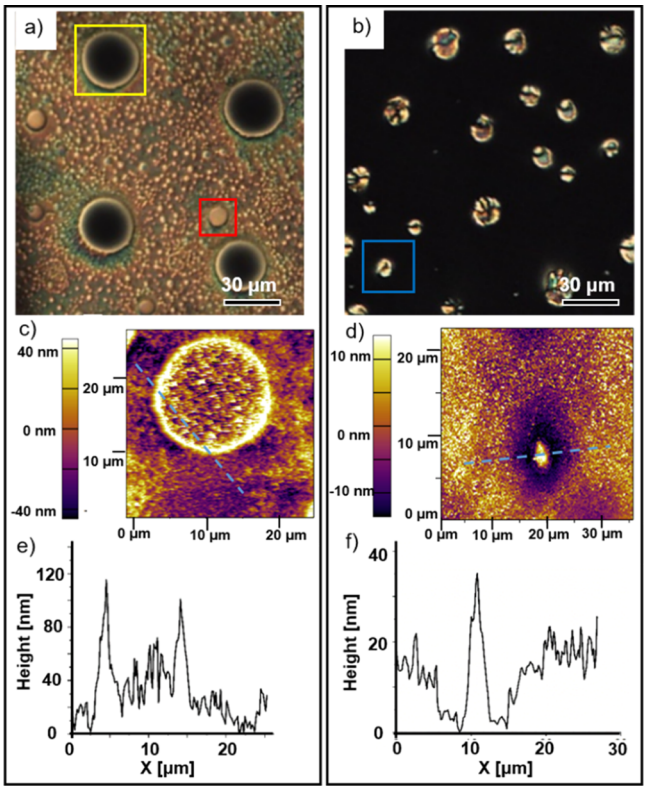

Figure 6. (a,b) 20 μm-thick LC films supported on (a) 140 nm-thick and (b) 50 nm-thick PBLG brush quenched with 10% chloroform in acetone showing (a) large circular homeotropic domains surrounded by continuous planar domain containing smaller circular domains with tilted LC anchoring (red inset) and (b) micrometer-scale circular domains with tilted LC anchoring (blue inset). (c,d) corresponding 2D AFM cross sections and (e,f) 2D height profiles (blue dashed lines) of (c,e) 140 nm and (d,f) 50 nm thick PBLG brushes, respectively.

orientation that reflects a local averaging of surface orienting forces, the circular domain with elevated topography (2 μm diameter; Figure 6f), which is surrounded by a ring-like region comprising collapsed PBLG cannot be resolved by the 20 μm-thick LC film. Additionally, the presence of circular domains exhibited by brushes pretreated with chloroform−acetone mixtures suggests that brush patterning is a consequence of the nucleation of either chloroform or acetone droplets at the brush interface (i.e., phase separation). While we do not yet understand why localized phase separation of chloroform and acetone occurs at the brush interface, we have observed similar phenomena in other mixed solvent systems (see Section S16).

4. CONCLUSIONS

In conclusion, this paper advances our understanding of how treatment of PBLG brushes with solvent induces brush organization and how PBLG brush organization impacts LC ordering. A combination of measurements performed using AFM, FTIR spectroscopy, and polarized light microscopy support the proposal that the ordering of LCs on PBLG brushes is dictated by the PBLG chain orientation, which in turn is regulated by the formation of teepee-like assemblies. Additional measurements using PBLG brushes of distinct thickness and subjected thermal denaturation provide support to our conclusions. We use these new insights to interpret the spontaneous patterning of PBLG brush organization induced by solvent mixtures.

The observations reported in this paper generate a number of unresolved questions. For example, we do not yet fully understand the physical processes that accompany the patterning of PBLG orientations by mixed solvents. Our results suggest that the phase separation of the mixed solvent (or, at least, the formation of solvent droplets with distinct compositions on the PBLG brush surface) leads to "coffee-stain"-type effects. It is also possible that energetic barriers to nucleation at the brush surface depend on brush composition and thickness and thus control droplet formation.[54−56]

Our results lay the groundwork for a number of directions for future exploration. For example, we envision studies that utilize mixed solvent-treated patterned polymer brushes to control the functional properties of surfaces. In particular, it may be possible to control the interactions of proteins with surfaces via manipulation of the organization of the PBLG brushes.[57−61] Alternatively, the phenomena reported in this paper might be exploited to tune size exclusion filters, in which polymer brush-decorated pores are reversibly modulated by pretreatment with solvent mixtures. We also envisage future studies that incorporate polymer brushes with a broadened range of chemical functionalities, such as those that engage in intermolecular interactions, which lead to reversible cross-linking.[62]

■ ASSOCIATED CONTENT

Supporting Information

The Supporting Information is available free of charge at https://pubs.acs.org/doi/10.1021/acs.macromol.1c01125.

PBLG molecular weight and grafting density calculation; estimation of the average PBLG tilt angle via FT-IR; LC tilt estimation; effect of PBLG brush pretreatment with 5CB on the PBLG tilt angle; LC response to initiator-functionalized substrates and PBLG thin films; PBLG brushes change the easy axis of LCs; 2D and 3D height profiles of PBLG brushes via AFM; LC response to PBLG brushes of variable thickness; probing intermolecular interactions between LCs and PBLG; relationship between LC and PBLG tilt angles; deconvolved FTIR spectra of heat-treated 130 nm-thick PBLG brushes; FTIR spectra of mixed solvent treated 140 nm-thick PBLG brushes; fractional area coverage of homeotropic domains in the LC film supported on 140 nm-thick PBLG brush treated with mixed solvents; 2D and 3D height profiles of 140 nm-thick PBLG brushes via AFM; 2D and 3D height profiles of 50 nm-thick PBLG brushes via AFM; and patterning of PBLG brushes via nucleation of chloroform at PBLG brush interfaces (PDF)

■ AUTHOR INFORMATION

Corresponding Authors

Christopher K. Ober − *Department of Materials Science and Engineering, Cornell University, Ithaca, New York 14853, United States*; Email: christopher.ober@cornell.edu

Nicholas L. Abbott − *Smith School of Chemical and Biomolecular Engineering, Cornell University, Ithaca, New York 14853, United States*; orcid.org/0000-0002-9653-0326; Email: nabbott@cornell.edu

https://doi.org/10.1021/acs.macromol.1c01125
Macromolecules 2021, 54, 7786−7795

Authors

Michael Tsuei − *Smith School of Chemical and Biomolecular Engineering, Cornell University, Ithaca, New York 14853, United States;* orcid.org/0000-0002-1748-4035

Hai Tran − *Smith School of Chemical and Biomolecular Engineering, Cornell University, Ithaca, New York 14853, United States*

Sangchul Roh − *Smith School of Chemical and Biomolecular Engineering, Cornell University, Ithaca, New York 14853, United States*

Complete contact information is available at: https://pubs.acs.org/10.1021/acs.macromol.1c01125

Author Contributions

M.T. and H.T. contributed equally to this work. All authors have given approval to the final version of the manuscript. This manuscript was written through contributions of all authors.

Notes

The authors declare no competing financial interest.

■ ACKNOWLEDGMENTS

We acknowledge support of this research from the Army Research Office through W911NF-15-1-0568 and W911NF-17-1-0575. We also acknowledge support of this research through the National Science Foundation, DMR-1905403. Additionally, this work was performed in part at the Cornell Nanoscale Facility, an NNCI member supported by NSF Grant NNCI-2025233 and the Cornell Center for Materials Research Shared Facilities which are supported through the NSF MRSEC program (DMR-1719875).

■ REFERENCES

(1) Li, M.; Pester, C. W. Mixed Polymer Brushes for. Smart" Surfaces. *Polymers* **2020**, *12*, 1553.

(2) Lemieux, M.; Usov, D.; Minko, S.; Stamm, M.; Shulha, H.; Tsukruk, V. V. Reorganization of Binary Polymer Brushes: Reversible Switching of Surface Microstructures and Nanomechanical Properties. *Macromolecules* **2003**, *36*, 7244−7255.

(3) Stuart, M. A. C.; Huck, W. T. S.; Genzer, J.; Müller, M.; Ober, C.; Stamm, M.; Sukhorukov, G. B.; Szleifer, I.; Tsukruk, V. V.; Urban, M.; Winnik, F.; Zauscher, S.; Luzinov, I.; Minko, S. Emerging Applications of Stimuli-responsive Polymer Materials. *Nat. Mater.* **2010**, *9*, 101−113.

(4) Jaworek, T.; Neher, D.; Wegner, G.; Wieringa, R. H.; Schouten, A. J. Electromechanical Properties of an Ultrathin Layer of Directionally Aligned Helical Polypeptides. *Science* **1998**, *279*, 57−60.

(5) Wang, Y.; Chang, Y. C. Preparation of Unidirectional End-grafted Alpha-helical Polypeptides by Solvent Quenching. *J. Am. Chem. Soc.* **2003**, *125*, 6376−6377.

(6) Zheng, Y.; Bruening, M. L.; Baker, G. L. Crystallization of Polymer Brushes with Poly(ethylene oxide) Side Chains. *Macromolecules* **2007**, *40*, 8212−8219.

(7) Snaith, H. J.; Whiting, G. L.; Sun, B.; Greenham, N. C.; Huck, W. T. S.; Friend, R. H. Self-Organization of Nanocrystals in Polymer Brushes. Application in Heterojunction Photovoltaic Diodes. *Nano Lett.* **2005**, *5*, 1653−1657.

(8) Page, Z. A.; Narupai, B.; Pester, C. W.; Bou Zerdan, R.; Sokolov, A.; Laitar, D. S.; Mukhopadhyay, S.; Sprague, S.; McGrath, A. J.; Kramer, J. W.; Trefonas, P.; Hawker, C. J. Novel Strategy for Photopatterning Emissive Polymer Brushes for Organic Light Emitting Diode Applications. *ACS Cent. Sci.* **2017**, *3*, 654−661.

(9) Ma, H.; Liu, M. S.; Jen, A. K.-Y. Interface-tailored and Nanoengineered Polymeric Materials for (Opto)electronic Devices. *Polym. Int.* **2009**, *58*, 594−619.

(10) Zou, Y.; Lam, A.; Brooks, D. E.; Srikantha Phani, A.; Kizhakkedathu, J. N. Bending and Stretching Actuation of Soft Materials through Surface-Initiated Polymerization. *Angew. Chem., Int. Ed.* **2011**, *50*, 5116−5119.

(11) Huck, W. T. S. Responsive Polymers for Nanoscale Actuation. *Mater. Today* **2008**, *11*, 24−32.

(12) Burkert, S.; Bittrich, E.; Kuntzsch, M.; Müller, M.; Eichhorn, K.-J.; Bellmann, C.; Uhlmann, P.; Stamm, M. Protein Resistance of PNIPAAm Brushes: Application to Switchable Protein Adsorption. *Langmuir* **2010**, *26*, 1786−1795.

(13) Chang, Y. C.; Frank, C. W.; Forstmann, G. G.; Johannsmann, D. Quadrupolar and Polar Anisotropy in End-grafted Alpha-helical Poly(gamma-benzyl-L-glutamate) on Solid Substrates. *J. Chem. Phys.* **1999**, *111*, 6136−6143.

(14) Lee, N. H.; Frank, C. W. Surface-Initiated Vapor Polymerization of Various Alpha-Amino Acids. *Langmuir* **2003**, *19*, 1295−1303.

(15) Tran, H.; Zhang, Y.; Ober, C. K. Synthesis, Processing, and Characterization of Helical Polypeptide Rod-Coil Mixed Brushes. *ACS Macro Lett.* **2018**, *7*, 1186−1191.

(16) Pan, C.-T.; Yen, C.-K.; Lin, L.; Lu, Y.-S.; Li, H.-W.; Huang, J. C.-C.; Kuo, S.-W. Energy Harvesting with Piezoelectric Poly(Gamma-Benzyl-Glutamate) Fibers Prepared Through Cylindrical Near-Field Electrospinning. *RSC Adv.* **2014**, *4*, 21563−21570.

(17) Machida, S.; Urano, T. I.; Sano, K.; Kato, T. Response of a Hydrogen-Bonded Liquid Crystal to an Applied Electric Field Accelerated by a Poly(gamma-benzyl L-glutamate) Chemical Reaction Alignment Film. *Langmuir* **1997**, *13*, 576−580.

(18) Yang, C.-T.; Wang, Y.; Chang, Y.-C. Effect of Solvents and Temperature on the Conformation of Poly(beta-benzyl-L-aspartate) Brushes. *Biomacromolecules* **2010**, *11*, 1308−1313.

(19) Wu, J.-C.; Chen, C.-C.; Chen, K.-H.; Chang, Y.-C. Controlled Growth of Aligned Alpha-helical-polypeptide Brushes for Tunable Electrical Conductivity. *Appl. Phys. Lett.* **2011**, *98*, 133304.

(20) Riou, S. A.; Hsu, S. L.; Stidham, H. D. Structural Study of Poly(beta-benzyl-L-Aspartate) Monolayers at Air-Liquid Interfaces. *Biophys. J.* **1998**, *75*, 2451−2460.

(21) Kyotani, H.; Kanetsuna, H.; Ōya, M. Conformational Transitions of Poly(beta-benzyl-L-Aspartate). *J. Polym. Sci.* **1977**, *15*, 1029−1036.

(22) Vlasova, E.; Volchek, B.; Tarasenko, I.; Vlasov, G. Spectroscopic Investigation of Polypeptide Plane Brushes. *Macromol. Symp.* **2011**, *305*, 116−121.

(23) Dazzi, A.; Prater, C. B.; Hu, Q.; Chase, D. B.; Rabolt, J. F.; Marcott, C. AFM-IR: Combining Atomic Force Microscopy and Infrared Spectroscopy for Nanoscale Chemical Characterization. *Appl. Spectrosc.* **2012**, *66*, 1365−1384.

(24) Popov, P.; Mann, E. K.; Jákli, A. Thermotropic Liquid Crystal Films for Biosensors and Beyond. *J. Mater. Chem. B* **2017**, *5*, 5061−5078.

(25) Bukusoglu, E.; Bedolla Pantoja, M.; Mushenheim, P. C.; Wang, X.; Abbott, N. L. Design of Responsive and Active (Soft) Materials Using Liquid Crystals. *Annu. Rev. Chem. Biomol. Eng.* **2016**, *7*, 163−196.

(26) Carlton, R. J.; Hunter, J. T.; Miller, D. S.; Abbasi, R.; Mushenheim, P. C.; Tan, L. N.; Abbott, N. L. Chemical and Biological Sensing Using Liquid Crystals. *Liq. Cryst. Rev.* **2013**, *1*, 29−51.

(27) Miller, D. S.; Wang, X.; Abbott, N. L. Design of Functional Materials Based on Liquid Crystalline Droplets. *Chem. Mater.* **2014**, *26*, 496−506.

(28) Mushenheim, P. C.; Abbott, N. L. Hierarchical Organization in Liquid Crystal-in-Liquid Crystal Emulsions. *Soft Matter* **2014**, *10*, 8627−8634.

(29) Fuster, H. A.; Wang, X.; Wang, X.; Bukusoglu, E.; Spagnolie, S. E.; Abbott, N. L. Programming van der Waals Interactions with Complex Symmetries into Microparticles using Liquid Crystallinity. *Sci. Adv.* **2020**, *6*, No. eabb1327.

(30) Biscari, P.; Turzi, S. Boundary-Roughness Effects in Nematic Liquid Crystals. *SIAM J. Appl. Math.* **2006**, *67*, 447−463.
(31) Kumar, S.; Kim, J. H.; Shi, Y. What Aligns Liquid Crystals on Solid Substrates? The Role of Surface Roughness Anisotropy. *Phys. Rev. Lett.* **2005**, *94*, 077803.
(32) Carlton, R. J.; Ma, C. D.; Gupta, J. K.; Abbott, N. L. Influence of Specific Anions on the Orientational Ordering of Thermotropic Liquid Crystals at Aqueous Interfaces. *Langmuir* **2012**, *28*, 12796−12805.
(33) Sato, K.; Yamasaki, T.; Nishide, H.; Oyaizu, K. Grafted Radical Polymer Brush for Surface-Driven Switching of Chiral Nematic Liquid Crystals. *Polym. J.* **2017**, *49*, 691−693.
(34) Li, X.; Yanagimachi, T.; Bishop, C.; Smith, C.; Dolejsi, M.; Xie, H.; Kurihara, K.; Nealey, P. F. Engineering the Anchoring Behavior of Nematic Liquid Crystals on a Solid Surface by Varying the Density of Liquid Crystalline Polymer Brushes. *Soft Matter* **2018**, *14*, 7569−7577.
(35) Hamelinck, P. J.; Huck, W. T. S. Homeotropic Alignment on Surface-Initiated Liquid Crystalline Polymer Brushes. *J. Mater. Chem.* **2005**, *15*, 381−385.
(36) Machida, S.; Urano, T. I.; Sano, K.; Kawata, Y.; Sunohara, K.; Sasaki, H.; Yoshiki, M.; Mori, Y. A Chiral Director Field in the Nematic Liquid Crystal Phase Induced by a Poly(gamma-benzyl glutamate) Chemical Reaction Alignment Film. *Langmuir* **1995**, *11*, 4838−4843.
(37) Urano, T. I.; Machida, S.; Sano, K. A New Variable Orienting Force for Liquid Crystals Which has its Origin in the Electric Property of Poly-gamma-benzyl-L-glutamate CRA Film. *J. Chem. Soc., Chem. Commun.* **1994**, 231−232.
(38) Urano, T. I.; Machida, S.; Sano, K. Dynamics of a Nematic Liquid Crystal on a PBLG-CRA Film. Time-Resolved Infrared Spectroscopic Study. *Chem. Phys. Lett.* **1995**, *242*, 471−477.
(39) Daly, W. H.; Poché, D. The Preparation of N-carboxyanhydrides of Alpha Amino Acids using Bis(trichloromethyl)carbonate. *Tetrahedron Lett.* **1988**, *29*, 5859−5862.
(40) Yadav, A. R.; Sriram, R.; Carter, J. A.; Miller, B. L. Comparative Study of Solution-Phase and Vapor-Phase Deposition of Aminosilanes on Silicon Dioxide Surfaces. *Mater. Sci.* **2014**, *35*, 283−290.
(41) Moon, J. H.; Shin, J. W.; Kim, S. Y.; Park, J. W. Formation of Uniform Aminosilane Thin Layers: An Imine Formation To Measure Relative Surface Density of the Amine Group. *Langmuir* **1996**, *12*, 4621−4624.
(42) Shircliff, R. A.; Stradins, P.; Moutinho, H.; Fennell, J.; Ghirardi, M. L.; Cowley, S. W.; Branz, H. M.; Martin, I. T. Angle-Resolved XPS Analysis and Characterization of Monolayer and Multilayer Silane Films for DNA Coupling to Silica. *Langmuir* **2013**, *29*, 4057−4067.
(43) Chang, Y.-C.; Frank, C. W. Vapor Deposition-Polymerization of alpha-Amino Acid N-Carboxy Anhydride on the Silicon (100) Native Oxide Surface. *Langmuir* **1998**, *14*, 326−334.
(44) Wieringa, R. H.; Siesling, E. A.; Geurts, P. F. M.; Werkman, P. J.; Vorenkamp, E. J.; Erb, V.; Stamm, M.; Schouten, A. J. Surface Grafting of Poly (L-Glutamates). 1. Synthesis and Characterization. *Langmuir* **2001**, *17*, 6477−6484.
(45) Kumar, P.; Oh, S. Y.; Baliyan, V. K.; Kundu, S.; Lee, S. H.; Kang, S.-W. Topographically Induced Homeotropic Alignment of Liquid Crystals on Self-Assembled Opal Crystals. *Opt. Express* **2018**, *26*, 8385−8396.
(46) Tripathi, P. K.; Pande, M.; Singh, S. Dielectric and Electro-optical Properties of Polymer-stabilized Liquid Crystal. II. Polymer PiBMA Dispersed in MBBA. *Appl. Phys. A* **2016**, *122*, 847.
(47) Kirov, N.; Simova, P.; Ratajczak, H. Influence of A.C. Electric Field on IR Spectra of Some Nematic Liquid Crystals with Positive and Negative Dielectric Anisotropy. *J. Mol. Struct.* **1978**, *46*, 487−493.
(48) Ushiki, H.; Mita, I. Study on the Fluorescence Depolarization of a Chromophore Attached to Polymer Chain End III. Aggregation and Helix-Coil Transition Behavior of Poly(gamma-benzyl L-glutamate) in m-Cresol and Benzene at Various Temperatures. *Polym. J.* **1985**, *17*, 1297−1300.
(49) EL-Mahdy, A. F. M.; Kuo, S.-W. Diphenylpyrenylamine-functionalized Polypeptides: Secondary Structures, Aggregation-induced Emission, and Carbon Nanotube Dispersibility. *RSC Adv.* **2018**, *8*, 15266−15281.
(50) Kotharangannagari, V. K.; Sánchez-Ferrer, A.; Ruokolainen, J.; Mezzenga, R. Thermoreversible Gel-Sol Behavior of Rod-Coil-Rod Peptide-Based Triblock Copolymers. *Macromolecules* **2012**, *45*, 1982−1990.
(51) Islam, S.; Velev, O. D. Mechanism and Control of "Coffee-Ring Erosion" Phenomena in Structurally Colored Ionomer Films. *Soft Matter* **2020**, *16*, 2683−2694.
(52) Denkov, N. D.; Velev, O. D.; Kralchevsky, P. A.; Ivanov, I. B.; Yoshimura, H.; Nagayama, K. Two-dimensional Crystallization. *Nature* **1993**, *361*, 26.
(53) Carrithers, A. D.; Brown, M. J.; Rashed, M. Z.; Islam, S.; Velev, O. D.; Williams, S. J. Multiscale Self-Assembly of Distinctive Weblike Structures from Evaporated Drops of Dilute American Whiskeys. *ACS Nano* **2020**, *14*, 5417−5425.
(54) Alberti, S.; Gladfelter, A.; Mittag, T. Considerations and Challenges in Studying Liquid-Liquid Phase Separation and Biomolecular Condensates. *Cell* **2019**, *176*, 419−434.
(55) Supriya, S.; Sushmitha, S.; Srinivasan, K. Effective Control of Liquid-Liquid Phase Separation and Nucleation of Vanillin Single Crystals through a Vapor Diffusion Crystallization Process in Selected Solvent Environments. *Cryst. Growth Des.* **2019**, *19*, 6315−6323.
(56) Nakagawa, S.; Yoshie, N. Periodic Surface Pattern Induced by Crystallization of Polymer Brushes in Solvents. *Macromolecules* **2020**, *53*, 8131−8139.
(57) Shanahan, H. P.; Garcia, M. A.; Jones, S.; Thornton, J. M. Identifying DNA-binding Proteins using Structural Motifs and the Electrostatic Potential. *Nucleic Acids Res.* **2004**, *32*, 4732−4741.
(58) Liew, C. K.; Simpson, R. J. Y.; Kwan, A. H. Y.; Crofts, L. A.; Loughlin, F. E.; Matthews, J. M.; Crossley, M.; Mackay, J. P. Zinc Fingers as Protein Recognition Motifs: Structural Basis for the GATA-1/Friend of GATA Interaction. *Proc. Natl. Acad. Sci. U.S.A.* **2005**, *102*, 583−588.
(59) Bulyk, M. L.; Huang, X.; Choo, Y.; Church, G. M. Exploring the DNA-binding specificities of Zinc Fingers with DNA Microarrays. *Proc. Natl. Acad. Sci. U.S.A.* **2001**, *98*, 7158−7163.
(60) Romero Romero, M. L.; Yang, F.; Lin, Y.-R.; Toth-Petroczy, A.; Berezovsky, I. N.; Goncearenco, A.; Yang, W.; Wellner, A.; Kumar-Deshmukh, F.; Sharon, M.; Baker, D.; Varani, G.; Tawfik, D. S. Simple yet Functional Phosphate-loop Proteins. *Proc. Natl. Acad. Sci. U.S.A.* **2018**, *115*, E11943−E11950.
(61) Jordan, P. W.; Saunders, N. J. Host Iron Binding Proteins Acting as Niche Indicators for Neisseria Meningitidis. *PLoS One* **2009**, *4*, No. e5198.
(62) Meersman, F.; Wang, J.; Wu, Y.; Heremans, K. Pressure Effect on the Hydration Properties of Poly(N-isopropylacrylamide) in Aqueous Solution Studied by FTIR Spectroscopy. *Macromolecules* **2005**, *38*, 8923−8928.

https://doi.org/10.1021/acs.macromol.1c01125
Macromolecules 2021, 54, 7786−7795